Barium boron aluminum silicate glass system for solid state optical gas sensors

M.J. Da Silva*, J. Karczewski[a], P. Jasinski[b], A. Chrzan[b], P. Kalinowski[b], D. Szymczewska[b], G. Jasinski[b]

*Universidade de São Paulo–IPEN, Av. Prof. Lineu Prestes 2242, São Paulo - SP, 05508-000, Brazil

[a]Gdańsk University of Technology, Faculty of Applied Physics and Mathematics, ul. Narutowicza 11/12, 80-233 Gdańsk, Poland

[b]Gdańsk University of Technology, Faculty of Electronics, Telecommunications and Informatics, ul. Narutowicza 11/12, 80-233 Gdańsk, Poland

Abstract

Recent increasing demand for new eco-friendly materials and for low cost fabrication process for use in optical sensors field, raise concern about alternative materials for this application. We have designed two glass-ceramics compositions from the quaternary RO-Al_2O_3-SiO_2-B_2O_3(R=Ba) alkali-earth aluminum silicate system, labeled B72 and B69, with high refractive index (>1.6), large values of Abbe number (94.0 and 53.0, respectively), and free of lead and arsenic. We present an analysis and discussion of experimental optical properties, thermal and thermo-chemical stability along with important properties such as transition temperature (T_g), onset of crystallization (T_x) as well transport properties as ionic conductivity behavior in the quaternary glass-ceramic system containing boron for use as optical sensors. Complex Impedance Spectra (Bode Plot) and Potentiodynamic Polarization curves (Tafel plots) measurements were carried out in the temperature range of 600 to 850ºC. The most probable conductivity mechanism is a thermally activated process of mobile ions overcoming a potential barrier (E_A), according to the Arrhenius regime. Here we report that charge transfer is caused by the flux of electrons, in the region of elevated temperatures (>700°C), and is affected by immiscibility of crystals, nucleation and growth type, that causes phase separation. We found conductivity (σ) values from 10^{-9} to 10^{-5} S/cm at temperatures between 700 and 850ºC. Our results highlight a need for research on ion mobility in the glassy network above the transition range, and the effect cause by metastable immiscibility in the alkaline-earth glasses are exposed. The two glass compositions B72 and B69 can be tailored by proper use as glassy optical sensor.

Keywords: Glass-ceramic; optical sensors; thermal stability; Impedance Spectroscopy; Arrhenius plot; Tafel plot

1. Introduction

Panoply of uses for glassy systems involves its optical properties. Application of glassy systems in the field of sensor materials remains limited. Consequently, the study and description of complex electrochemical processes and interaction between amorphous structure and physical-chemical properties offers potentially new opportunities. Optical sensors have advantages over their electrical counterpart as they can operate without any interference from surrounds electric or magnetic fields. They have fast response time as compared to electrical sensors and do not need electrical contacts that could be damaged by the monitored target. For the same reason, they are much safer in case of flammable gas and/or vapors[1].

In many applications, glass must serve as an electrical insulator or conductor, and therefore the understanding of its conductivity is important. In the majority of silicate oxides glasses, the electrical conductivity results from ionic motion of monovalent cations. Even in glasses with no nominal addition of monovalent ions, the conductivity results from transport of monovalent cations. For some types of gas sensors, such as fiber-optics, based on fluorescence effect, the conductivity is not a controlled parameter. Therefore no restrictions on conductivity of the designed materials is necessary[2].

The major interest about barium oxide based glasses lies on four reasons: (i) the high atomic weight of Ba^{2+} and (ii) its high polarizability which contributes greatly to increase the density, and including others properties as: chemical, thermal stability, and glass refraction index, (iii) Ba^{2+} strongly absorbs gamma rays, X-rays, and is non-toxic as compared to another heavy metal oxide ions such lead[3] (iv) finally, the conductivity of alkaline earth silicates should be consider(~2.10^{-7} S/cm at 550°C) and is affected by the presence of OH^- groups, and seems plausible that hydrogen ions are able to carry the electrical current in these glasses. It is also possible that the mobility of protons is higher in the alkaline earth, lead and some aluminum silicate glasses.

14th International Conference on Optical and Electronic Sensors, edited by Piotr Jasiński, Proc. of SPIE Vol. 10161, 101610G · © 2016 SPIE
CCC code: 0277-786X/16/$18 · doi: 10.1117/12.2248373

The herewith proposed low-cost system designed for optical sensor application can operate even in corrosive environments, and under radiation. Certain components in a glass can enhance optical nonlinearity at expense of severe environment impact. Common examples are the heavy metal ions giving high refractive index in the typical led, and bismuth based glass systems [4]. In this context, glass systems based on alkaline earth-metals oxides such as BaO can be used for H_2, and CO detection using refractive index variations.

The present work is an attempt to study the use of barium boron aluminum silicate glasses a stable, and eco-friendly glass system, lead and alkaline-free, with high Ba^{2+}content (~70%wt), displaying high refractive index (η=1.6) belong to BaO-Al_2O_3-SiO_2 system with B_2O_3. The batch compositions exhibits the same characteristics in comparison with well know trade names glasses compositions and most important: we have modified our raw materials and processes to be eco-friendly (lead and arsenic free) [5].

This study addresses three relevant points: 1) discuss the thermal stability and optical properties, 2) characterize the ionic transport and electrochemical properties using the Impedance Spectroscopy and Potentiodynamic polarization curves at high temperatures, and 3) states a new glass-ceramic composition for use as optical sensors.

2. Experimental

The chemical compositions of the investigated glass-ceramics are listed in Table 1. The compositions labeled B72 and B69, were used as basic glasses, and different amounts of B_2O_3 were introduced to replace SiO_2 in the parent glasses according to phase diagram relationships [6].The amount of Al_2O_3 has an effect on the thermal properties of the glass up to 5.0 %(wt). Exceeding this value leads to uncontrolled crystallization of glass under cooling. The content of the B_2O_3, as a flux agent, was limited at 9.0 % (wt) maximum, because boron content it is detrimental to the dielectric properties[7].

Analytical reagent graded $Ba(OH)_2$, Al_2O_3, silica SiO_2, and boric acid H_2BO_3 from Sigma-Aldrich(purity 99.9%), were used to prepare the glasses. The starting raw materials were mixed for 60 min in a ball mill, and then transferred to an alumina crucible and molten in the temperature range of 1400°C with a dwell time of 2h. The glasses obtained were crushed and milled in dry conditions in a rotating mill using agate containers and agate balls, for 2 h to obtain a fine glass powder (~50 to 70µm).

The glass-ceramic powders were then subjected to XRD phase analysis(not shown),using Bruker D8 model diffractometer with CuKα radiation (λ=1.54Å), for 2θ ranging between 10 and 80°, at a scanning speed of 0.02°/s, to confirm their amorphous nature. The refractive index was obtained by spectral-ellipsometry using an ellipsometer and we used the three-oscillator Sellmeier equation to estimate η. The characteristics temperatures (T_g,T_x), shown for each composition in Table 2, were determined by Differential Thermal Analysis (DSC) according to Da Silva *et al* [7].

After thermal treatment (800ºC for 2 h), Impedance Spectroscopy and conductivity measurements were carried using a Novocontrol High-resolution Dielectric analyzer in a frequency range from 1Hz to 1MHz with a voltage excitation of 3.0 V, and temperature ranging from 600 to 850°C. The microstructure of the glass-ceramic were investigated by scanning electron microscopy (FEI QUANTA FEG 250). Potentiodynamic polarization curves (Tafel plots) were performed on an electrochemical workstation Gamry Interface 1000 Potentiostat/Galvanostat/ZRA. A three-electrode cell was employed[8], with platinum electrode as the reference and the counter-electrode (both attached to YSZ ($Y_{0.16}Zr_{0.84}O_2$) 100 µm thick substrate), and the glass on YSZ as the working electrode. The polarization rate was 10 mV/s, scanning from -1.0 V *vs* OCP(open circuit potential) to +1.0 V *vs* OCP. The working electrode exposed area was ~0.5 cm^2.

Table 1 Batch compositions and optical properties: refractive index, η(at 486.1 nm), Abbe(υd) number [5]

Glass	Composition (wt %)				Optical Properties	
	BaO	Al_2O_3	SiO_2	B_2O_3	η (at 468.1 nm)	υ_d
B72	72	4.5	20.5	3	1.62	94.0
B69	69	4.5	17.5	9	1.62	53.0

Table 2 Characteristics temperatures of the glass ssmples: T_g=glass transition; defined here as the onset of glass transition, T_x= onset of crystallization, and $\Delta T_x=(T_x-T_g)/T_g$ [7]

Glass	Characteristics temperatures(°C)		ΔT_x(%)
	T_g	T_x	
B72	678	857	26
B69	680	758	11

3. Results and discussion

The goal of current study was to determine key properties in research and development of gas sensors that determine the best design: morphology, thermo-stability, and electro-chemical properties.

3.1 Phase separation

There are basically two mechanisms by which phase separation can occurs in glasses: *spinodal* decomposition(or interconnect) and nucleation/growth[9], where the center of the bimodal dome is the region of the *spinodal* decomposition (yellow region Figure 1a: II and III). In contrast to the nucleation region, the *spinodal* decomposition (region I Figure 1a) is a thermodynamically driven process where spontaneous separation of a homogeneous solution or melt into two distinct phases occurs and there is no activation energy barrier. However, in our case no glass compositions fall into the region where the second mechanism termed s*pinodal* occurs Figure 1: b (B72) and c (B69).

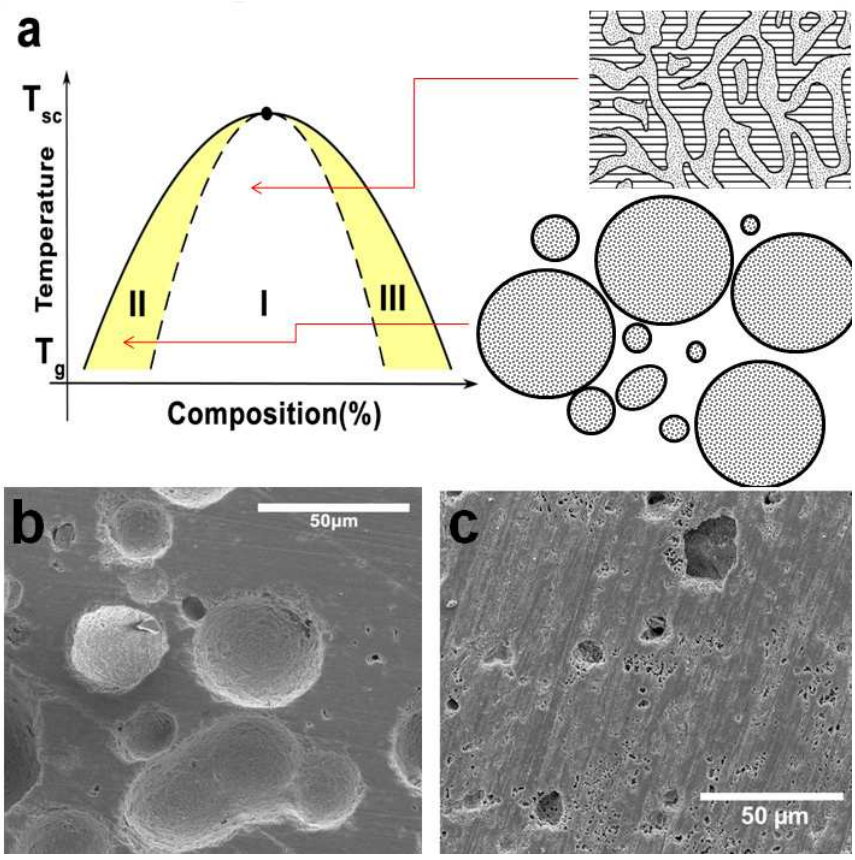

Figure 1 (a) Schematic phase diagram showing zones of liquid-liquid immiscibility and its phases boundary in a glassy composition. Where: Tsc is the superior consolute temperature: temperature above which the liquid mixture does not separate into two phases for any given composition, and Tg: glass transition temperature [10];(b) B72 and (c) B69 samples.

In view of those considerations, one can discuss the microstructural features of glasses in the system $BaO\text{-}SiO_2\text{-}Al_2O_3$ with B_2O_3addition. The miscibility gap for this system is metastable as it is shown in Figure. 1(a). For our compositions on the barium rich side, the microstructure consisted of droplet-shaped SiO_2 –rich particles immersed in a continuous BaO-rich matrix. There is no debate that morphology of a sample can affect the glass conductivity, the alkaline-earth modifier ion helps to create isolated spheres distributed in a matrix of a much lower conductivity phase. This morphology is shown more explicitly in Figure 1(b) for B72 glass.

The glass forming region was chosen at the *subsolidus* region of the $BaO–Al_2O_3–SiO_2$ system (Fig.2) within the compatibility triangle (BS–B2S–BAS2) because the nature of the crystals that formed on heat treatment of an individual glass composition can be predicted from the phase diagrams [9]. The following phases have been characterized by X-ray diffraction patterns: JCPDS 27-1035: barium silicate-orthorhombic ($BaSiO_3$), JCPDS 00-027-10135: barium silicate-monoclinic ($2BaO.SiO_2$), JCPDS 01-077-0185: Celsian-hexagonal ($BaAl_2Si_2O_8$), and JCPDS 00-038-1450: Celsian (monoclinic); as expected according to phase equilibria relations (Fig.2).

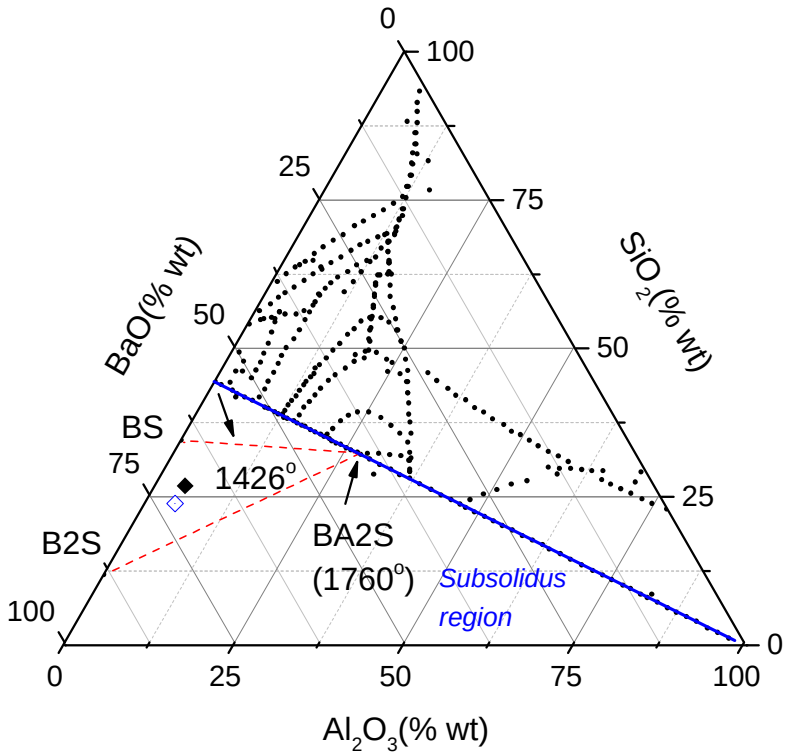

Figure 2 $BaO–Al_2O_3–SiO_2$ ternary equilibrium diagram showing the glass forming region for BAS glasses with batch compositions (the white rhombus represents B72 and the black one B69) and the compatibility triangle (BS–B2S–BAS2). B=BaO, $A=Al_2O_3$, $S=SiO_2$. [11].

3.2 Optical properties

In Table 1, it is possible to verify the dispersion values represented by the Abbe number according to $\upsilon_d=(\eta_d-1)/(\eta_F-\eta_C)$ for the B72 and B69 glasses. The dispersion was defined here as the difference between the refractive index measured at the F (486.1nm) and C (653.3 nm) emission lines of hydrogen, and the d line is related with the helium emission at (587.5 nm). Using this approach we found large Abbe number (up to 60), and considerable high refractive index (1.6) allow classifying the B72 and B69 samples as dense and extra dense barium crown glasses. Additionally, they display larger values of the Abbe parameter probably due to the presence of Al_2O_3 a former oxide which allows a homogeneous packing in the atomic network. The barium influence on the optical properties can be described as: (i) it increases the refractive index, due to its large size (stuffing effect), and (ii) it simultaneously reduces the dispersion in

the optical spectral region. This may occur due to its large electron density, as a result Ba^{2+} enlarges the transparency window and at the same time reduces the dispersion (Tab.1).

3.3 Thermal stability

Glass stability (Table 2) is the resistance towards crystallization[12] during reheating of the glass, and becomes important in our case involving remodeling a glass already done. Glass stability is normally characterized by the difference between the onset of crystallization (T_x) and the transition temperature (T_g). In particular, for the B72 and B69 samples heated at a linear heating rate (10 °C/min) we can compare the behavior of the samples which crystallize in very different conditions of rate and range of temperatures (Tab 2). As a result, we can observe that B72 glass is relatively more stable (26%) in comparison with the sample B69 (11%). To a detectable extent the determination of the crystal growth for the B69 glasses as a function of temperature can be seen by the micrograph showed in the Figure 1 (c). Where, the effects of the crystal structures on the glass formation is clear in terms of a significant number of crystals formed, in contrast with the B72 sample (Figure 1(a)).

3.4 Electrochemical stability at high temperatures

The Tafel curves depicted in the Figure 3, for the B72 and B69 glassy system, are dependent on the temperature of each assay. The electrochemical reactions were not easily observed because of the small velocity which the ions react to the driving forces: gradients of potential, concentration gradient, temperature gradient and last but not least the active-to-passive transition[13]. Those can be the main reasons for the slow rates with which glasses react with contacting solid, liquid phases, and even gaseous phases.

The values obtained for the corrosion current density (i_{corr}) at the glass transition point (T_g) are in the same order of magnitude (~10^{-7}A/cm^2) indicating resilience to dissolution process. The open circuit potential (OCP) or corrosion potential remains constant at the proximity of E=0.0V with the increasing temperature, suggesting a mixing control mechanism for the corrosion process. As shown in Figure 3, the exchange current density (i_0) increases from 4.0 10^{-7} to 1.7 10^{-4}A cm^{-2} with increasing temperature from glass transition (T_g) to onset of crystallization (T_x), respectively, for B72 sample. The parameter (i_0) gives an indication about how fast the reactions occur.

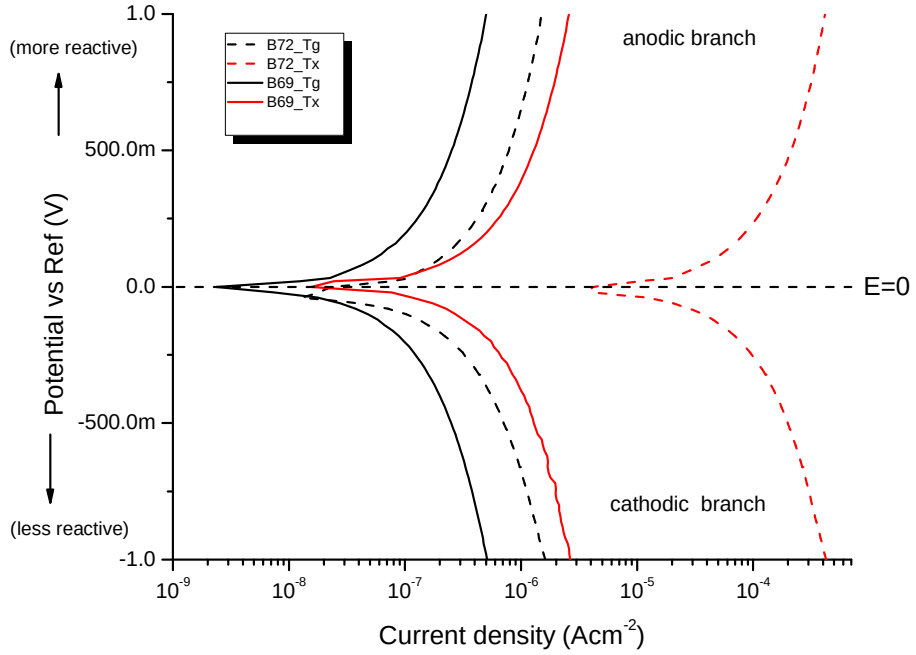

Figure 3 Potentiodynamic polarization curves for B72 and B69 glass samples at two characteristics temperatures T_g and T_x(*vide* Tab 1). Reference electrode: Pt

We must be aware that these reactions are complicated processes due to the glass structure, which consists of a network of forming elements and oxygen and modifying cations (Ba^{2+}), which are the slow charge carriers. In addition to the cations, also the network can react with components of contacting phases upon heating [14]. It seems that low thickness coatings induce a change in the surface reactivity, possibly due to the presence of defects in the glass layer or to a lack of homogeneousness of the layer. The defects might be related, as well, to the presence of droplet- shaped[15] (nucleation and growth type) immiscibility (Fig.1 (b)).

Commonly, in the study of ceramic materials by impedance spectroscopy (Fig. 4 and 5), phenomena that occur at high frequencies are attributed to the driving processes through the grains, while phenomena occurring at low frequencies to conduction at grain boundaries. In the particular case of glass-ceramics, that do not exhibit periodicity, symmetry, and long range ordering but at the same time, exhibits heterogeneities in structure, such as: density gradients, segregation, and phase separation that are related to the long range ordering phenomena, we can also attribute the impedance magnitude at high frequencies to the grain properties and the one at low frequencies to the grain boundary. The structure of the grain boundary is most resistive and thus predominant in conduction mechanisms for glass-ceramics. At this point (T_x), the glass-ceramic begin to form crystals with size enough to be detected by XRD (>30 Å)[16].

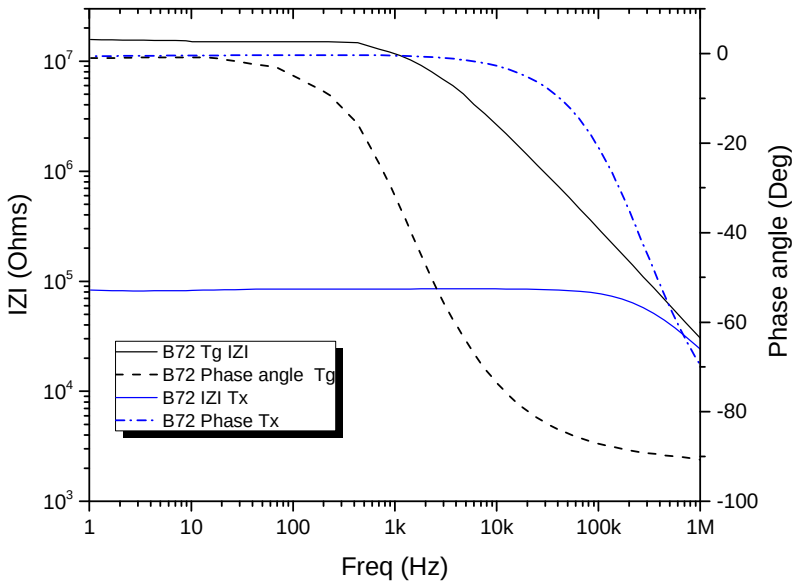

Figure 4 Bode plots of EIS spectra of B72 glass system exposed to temperatures equivalents to glass transition(T_g) and onset of crystallization (T_x), solid lines are plots of Z modulus (left axis) and Phase angle/Theta (right axis), *vs.* Frequency.

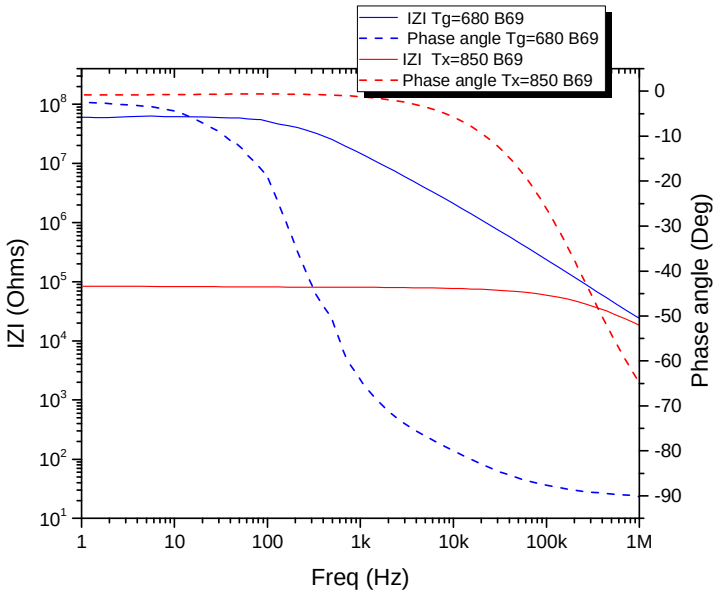

Figure 5 Bode plots of EIS spectra of B69 glass system exposed to temperatures equivalents to glass transition(T_g) and onset of crystallization (T_x), solid lines are plots of Z modulus (left axis) and Phase angle/Theta (right axis), *vs*. Frequency.

As temperature increase ((T_g to T_x), the impedance modulus in the low frequency range (<100 kHz) remains constant suggesting no changes in the structure within the measurement time (Figure 4 and 5). Despite, the impedance modulus seems to be not very different in respect to each other (B72 and B69). The phase angle plots may indicate the amorphisation level of the glass, which is visible as a shift to the higher frequency of the phase angle hump. This phenomenon is more pronounced for the B72 sample, due to structural relaxations process. The "defects" (comparing to ordered crystalline materials), or phonons, which scatter the electrons during their motions in an applied field, plays the role for impedance-vs-temperature behavior shown for the glassy material samples[17]. The phonon-assisted tunneling (hopping) from one localized state to another can occurs, but as expense of a great amount of energy (*vide* Figure 6) to overwhelm the energy barriers even at high temperatures (around T_x).

The mentioned shift in the phase angle for B72 sample (Fig.4) compared to the B69 (Fig.5), probably is related to the glass structure and immiscibility effects, associated to the response of the glassy substrate to the increasing temperature. These results validate the analysis illustrated in the Table 2, where previous results [5] show that the resistance to crystallization during heating (ΔT_x) for the B72 (26%) was almost two times greater than B69 (11%).

3.5 Ionic conductivity

Figure 6 shows the dependence of the conductivity of the glass ceramics with temperature in Arrhenius plot type with thermally activated behavior. The conductivity from 10^{-9} to 10^{-5} S/cm at temperatures between 600 and 850 ºC, exhibiting two main regions: a low(around T_g) and a high-temperature(vicinity of T_x) region. At high-temperature, the grain boundary activation energy (higher activation energy regions) relates to the onset of crystallization and rises up to 3.56 eV (BAS-7 sample) and 4.93 eV (B72). The two curves cross over at 800°C, point where the resistivity of grain interior is equal to the resistivity of the grain boundary. The B72 and B69 glass samples show a non-ordinary slope in the region above the glass transition temperature (T_g). This slope decreases as the temperature is lowered below T_g and a linear behavior is observed at lower temperatures (<750 °C) for both samples: B72 and B69. Therefore, implying a temperature-dependent activation energy (E_a) for the ionic charge transport. However, for B69 sample, a constant activation energy (E_a) from 770 °C to T=850 °C can be seen.

In the Arrhenius plot (Fig. 6) between the low and high temperature regions an intermediate regime occurs. Consequently, for this specific composition(B72) we can identify three distinct regimes: around T_g, a fit with the Arrhenius equation law results in activation energies equal to 1.6 eV, and at temperatures above 750 °C exhibit activation energies around 2.7 eV, and up to 800°C (4.93 eV) which can be related to conductivity measurements of fully crystallized $BaAl_2Si_2O_8$ ceramics[18].

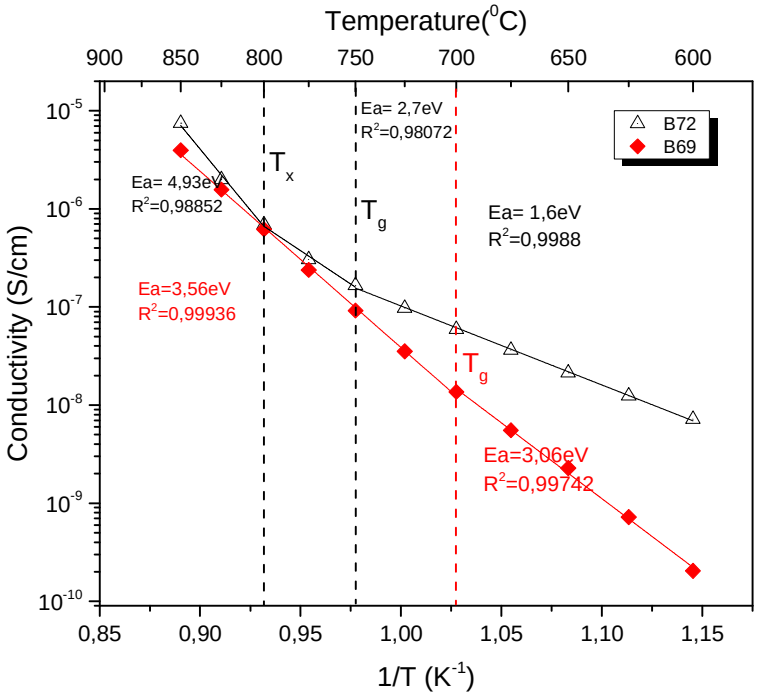

Figure 6 DC conductivity *vs.* 1000/T showing a quasi-Arrhenius behavior for the B72 and B69 glassy samples. Red and black lines are Arrhenius local fitting in temperature ranges where activation energies are calculated *vs* 1/ T plots.

However, authors also observed that additions of alumina do not exert a strong effect on the conductivity, but that Ba^{2+} ions participate markedly in the ion migration and transfer mechanisms when more than 10%(wt) BaO are present[19]. The O^{2-} ion migration is presumed to be the most decisive factor in this case, since the activation energy decreases in proportion with the increase in numbers of non-bridging oxygen atoms and, also, in residual OH^- group content.

These results are in agreement with previously reported [5] NMR spectra of the studied glasses, which contain basically Q1 (short chains) and Q2 (dimers) units in the glass network (B72 exhibited at least three times more units than B69), instead of stressed rigid and polymerized Q4 (the superscript means the number of bridging oxygens). Malki *et al.* [20] suggested that this kind of "floppy" structure has an increased mobility of the network modifier (Ba^{2+}) and has a consequence the increased total conductivity. Consequently, the glass transition occurs when the free volume is sufficient to reduce the stress caused by structural accommodation. We can suggest that the slope in the Arrhenius plot arises from a combination of factors like high modifier oxide content (BaO), a huge amount of dimmers (Q2), the motion of the more mobile B^{3+} ions, and the temperature-dependent local changes in the glass structure.

4. Conclusions

Glass-ceramic materials belonging to the quaternary system $BaO\text{-}Al_2O_3\text{-}SiO_2\text{-}B_2O_3$, have been studied as a potential glass sensor using modified process and low cost eco-friendly batch materials (lead and arsenic free), and at the same time with similar characteristics in comparison with traditional compositions: high refractive index (>1.6) and large values of Abbe number: 53.0 (B72) and 94.0 (B69).The results for the interfacial activation energy shows that the ions move across the glassy phase and after that reach diffusion pathways. There is a strong relationship between structure (vitreous state, immiscibility) and the ionic conductivity. The transition glassy to crystal state is related with changes on mobility of charge carries and to the accommodation of the structural units (relaxation). This effect is clearly demonstrated in Fig.6. The electrochemical measurements (Bode plot) indicated the level of amorphisation of the glass which results in an enlargement of the phase angle peak to the middle to low frequency range related to structural

relaxations process as transition temperature range. The maximum value of the impedance magnitude in the low frequency range remains constant (around 100 kΩ) indicating stability at high temperature (>800°C). Tafel curves indicated slow rates of dissolution at glass transition point ($\approx 10^{-7}$ A/cm^2). The two compositions labeled B72 and B69 can be properly tailored for use as glassy optical sensor, further investigations and measurements at the transition between glassy and the onset of crystallization temperature will be investigated.

Acknowledgements

This work was financed by the Brazilian government through the National Scientific Funding Agency CNPq (*Conselho Nacional de Desenvolvimento Científico e Tecnológico*), as part of the Science without Borders (CsF-PDE) fellowship program (Project No 233658/2014-9).

References

[1] Blank, T. A., Eksperiandova, L. P.., Belikov, K. N., "Recent trends of ceramic humidity sensors development: A review," Sensors Actuators B Chem. **228**, 416–442, Elsevier B.V. (2016).

[2] Traversa, E., "Ceramic sensors for humidity detection: the state-of-the-art and future developments," Sensors Actuators B Chem. **23**(2-3), 135–156 (1995).

[3] Navarro, J. M. F., El vidrio, E. CSIC, Ed., CSIC Press, Madrid (2003).

[4] A. Paul., Chemistry of Glasses, 2nd ed., Springer (1989).

[5] Da Silva, M. J., Moya, J. S., Pecharromán, C., Sanz, J., Mello-Castanho, S., "High barium content lead and alkaline-free glasses," Mater. Lett. **136**, 345–348, Elsevier (2014).

[6] Levin, E. M., Phase diagrams for ceramists, 50th ed., E. M. Levin, C. R. Robbins, H. F. McMurdie, and M. K. Reser, Eds., American Ceramic Society (1964).

[7] Da Silva, M. J., Bartolomé, J. F., De Aza, A. H.., Mello-Castanho, S., "Glass ceramic sealants belonging to BAS (BaO–Al2O3–SiO2) ternary system modified with B2O3 addition: A different approach to access the SOFC seal issue," J. Eur. Ceram. Soc. **36**(3), 631–644, Elsevier Ltd (2016).

[8] Szymczewska, D., Karczewski, J., Chrzan, A.., Jasinsky, P., "Three electrode configuration measurements of electrolyte-diffusion barrier-cathode interface," J. Ceram. Soc. Japan **123**(1436), 268–273 (2015).

[9] Jiang, Z.-H.., Zhang, Q.-Y., "The structure of glass: A phase equilibrium diagram approach," Prog. Mater. Sci. **61**, 144–215 (2014).

[10] Levin, E. M.., Cleek, G. W., "Shape of Liquid Immiscibility Volume in the System Barium Oxide-Boric Oxide-Silica," J. Am. Ceram. Soc. **41**(5), 175–179 (1958).

[11] Semler, C. E.., Foster, W. R., "System BaO-Al2O3-SiO2. IV. The System Celsian-Alumina and the Join Celsian-Mullite," J. Am. Ceram. Soc. **52**, 679–680 (1969).

[12] Shelby, J. E., Introduction to Glass Science and Technology, The Royal Society of Chemistry (2005).

[13] W. J. van Ooij, D. Zhu, M. Stacy, A. Seth, T. Mugada, J. Gandhi, P. P., "Corrosion Protection Properties of Organofunctional Silanes —An Overview," TSINGHUA Sci. Technol. **10**(6), 639–664 (2005).

[14] Wang, D. P., Wang, S. L.., Wang, J. Q., "Relationship between amorphous structure and corrosion behaviour in a Zr–Ni metallic glass," Corros. Sci. **59**, 88–95 (2012).

[15] Kukizaki, M., "Large-scale production of alkali-resistant Shirasu porous glass (SPG) membranes : Influence of ZrO 2 addition on crystallization and phase separation in Na 2 O – CaO – Al 2 O 3 – B 2 O 3 – SiO 2 glasses ; and alkali durability and pore morphology of the," J. Memb. Sci. **360**(1-2), 426–435, Elsevier B.V. (2010).

[16] Smiljanić, S. V., Grujić, S. R., Tošić, M. B., Živanović, V. D., Stojanović, J. N., Matijašević, S. D.., Nikolić, J. D., "Crystallization and sinterability of glass-ceramics in the system La2O3–SrO–B2O3," Ceram. Int. **40**(1), 297–305 (2014).

[17] Henisch, H. K., "The physics of amorphous solids," Mater. Res. Bull. **18**, 1584–1585 (1983).

[18] Lee, K. T.., Aswath, P. B., "Kinetics of the hexacelsian to celsian transformation in barium aluminosilicates doped with CaO," Int. J. Inorg. Mater. **3**, 687–692 (2001).

[19] Chandra, A., Bhatt, A.., Chandra, A., "Ion Conduction in Superionic Glassy Electrolytes: An Overview," J. Mater. Sci. Technol. **29**(3), 193–208, Elsevier Ltd (2013).

[20] Malki, M., Micoulaut, M., Chaimbault, F., Vaills, Y.., Simon, P., "Percolative conductivity in alkaline-earth silicate melts and glasses," Europhys. Lett. **64**(5), 661–667 (2003).